Design and characterization of a nonuniform linear vertical-cavity surface-emitting laser array with a Gaussian far-field distribution

Jinjiang Cui,[1,2,3] Yongqiang Ning,[1,*] Yan Zhang,[1,3] Peng Kong,[3] Guangyu Liu,[1,3] Xing Zhang,[1,3] Zhenfu Wang,[1,3] Te Li,[1,3] Yanfang Sun,[1] and Lijun Wang[1]

[1]Key Laboratory of Excited State Processes, Changchun Institute of Optics, Fine Mechanics, and Physics, Chinese Academy of Sciences, 16 Eastern South Lake Road, Changchun 130033, China

[2]Suzhou Institute of Biomedical Engineering and Technology

[3]Graduate School of Chinese Academy of Sciences, Beijing 100039, China

*Corresponding author: ningyq@ciomp.ac.cn

Received 17 February 2009; revised 21 May 2009; accepted 27 May 2009; posted 28 May 2009 (Doc. ID 107663); published 10 June 2009

A 980 nm bottom-emitting vertical-cavity surface-emitting laser array with a nonuniform linear arrangement is reported to realize emission with a Gaussian far-field distribution. This array is composed of five symmetrically arranged elements of 200 μm, 150 μm, and 100 μm diameter, with center spacing of 300 μm and 250 μm, respectively. An output power of 880 mW with a high power density of 1 kW/cm^2 is obtained. The divergence angle is below 20° in the range of operating current from 0 A to 6 A. The theoretical simulation of the near-field and the far-field distribution is in good agreement with the experimental result. The comparison between this nonuniform linear array, the single device, and the conventional two-dimensional array is carried out to demonstrate the good performance of the linear array.

OCIS codes: 140.7260, 140.1240, 140.3295.

1. Introduction

Dramatic improvements in vertical-cavity surface-emitting laser (VCSEL) performance have been obtained due to advances in fabrication techniques for optical and electrical confinement, as well as in the design of quantum well structures and the growth of Bragg mirrors. Nowadays, VCSELs with small diameter (less than 20 μm) and low output power have been widely used in optical communications, scanning, and massive parallel optical interconnections [1–3]. The applications in solid-state laser pumping, numerous medical applications, high-resolution printing, and free-space optical data communication are revealing a growing market for high-power diode lasers [4–6]. To increase the overall optical output power, the lasing area of the device has to be enlarged. One way is to increase the active area of single devices. However, the power conversion efficiency from electric power to optical power will be decreased with increasing active area, which limits a further increase of the active area. Alternatively, VCSELs are easy to integrate into arrays on a single chip with the merits of simple structure, high array density, high power, and easy heat extraction. But, the circle or ring beams of individual elements in a conventional two-dimensional (2D) array will superimpose and form a periodic intensity distribution with a series of peaks at far field. This poor far-field distribution and the necessity of a complex beam shaping system will limit further increasing of the lasing power.

In this paper, a nonuniform linear VCSEL array consisting of five elements with different diameters

0003-6935/09/183317-05$15.00/0

and center spacings is presented. In this linear array, the central element has the largest diameter, with the diameter and the center spacing of the second and the third adjacent elements decreasing in sequence. The purpose of this arrangement is to obtain a compromise among the output power, the power conversion efficiency, and the operation current of the array. With an optimized arrangement, an output power of 880 mW with a high power density of 1 kW/cm^2 is achieved. A good beam property of Gaussian far-field distribution is demonstrated. The comparison of the performances among this linear array, a single device, and the conventional 2D, 4 × 4 array is carried out to demonstrate the good performance of the nonuniform linear array.

2. Device Structure and Process

A schematic cross-section view of a VCSEL structure is shown in Fig. 1. The epitaxy wafer is grown on (100) GaAs substrate by using low-pressure metal organic chemical vapor deposition (MOCVD). The carbon-doped p-type distributed Bragg reflector consists of 30 pairs of $Al_{0.9}Ga_{0.1}As/GaAs$ with a graded interface to reduce series resistance. The n-type Si-doped Bragg stack consists of 28 pairs of the same material composition providing 99.3% reflectivity. The active region with an emission wavelength of about 980 nm is composed of three 8 nm thick $In_{0.2}Ga_{0.8}As$ quantum wells, 10 nm thick GaAs barriers, and AlGaAs claddings to form a one-λ cavity. A 30 nm thick AlAs layer is inserted between the p-type cladding layer and the p-side distributed Bragg reflector (DBR) for selective oxidation to provide lateral current confinement.

After a wet chemical etching of the mesa down to the depth of the AlAs layer, the AlAs layer is laterally oxidized for 30 minutes at 420 °C under nitrogen gas bubbled through water at 90 °C to form the current apertures with the oxidation depths from 20 to 30 μm. A SiO_2 passivating layer is deposited on the mesa to avoid short circuits when the device is p-side down soldered on a heat sink. After selective etching of the SiO_2 film, TiPtAu is evaporated on the mesa by using electron beam deposition. Before depositing an antireflection (AR) coating of HfO_2, the substrate is thinned and polished to a thickness of 150 μm in order to reduce absorption losses. An emission window is then formed on the bottom of the GaAs substrate, which is surrounded by large-area AuGeNi/Au contacts. The annealing is carried out at 420 °C in a nitrogen environment for 60 seconds. Devices are cleaved and then soldered junction-down with AuSn solder on a metallized diamond heat spreader. The diamond heat spreader is attached with In paste on a copper submount for measurement.

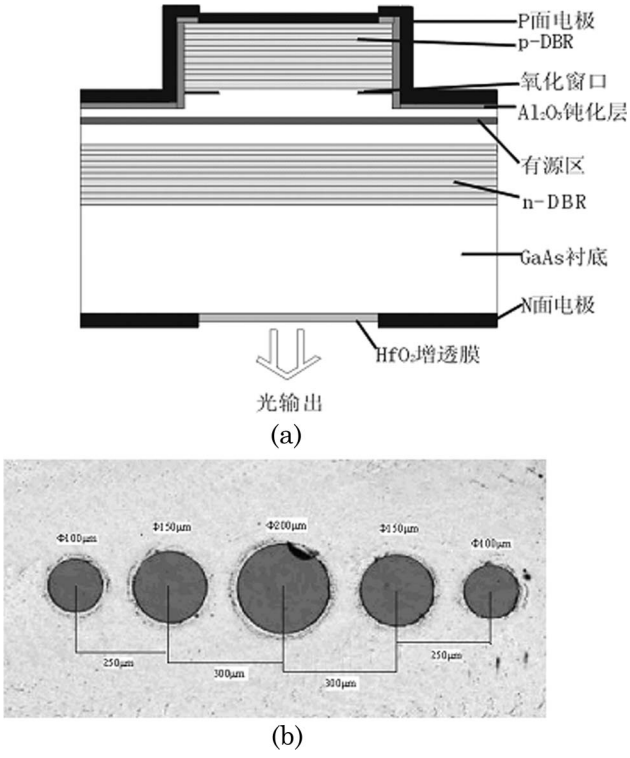

Fig. 1. Schematic diagram of (a) bottom-emitting VCSEL and (b) nonuniform linear array.

3. Simulation of Near-Field and Far-Field Distributions

The arrangement of the nonuniform linear array is depicted in Fig. 1, which is composed of five symmetrically arranged elements with 200 μm, 150 μm, and 100 μm diameter, and 300 μm and 250 μm center spacing, respectively. The laser beam of each large aperture-size unit has a multimode Hermite–Gaussian distribution. Assuming the distributions of the modes are independent of each other, the superposition of multimode Hermite–Gaussian distribution is applied on the x–z plane. The relationship between a multimode Gaussian beam and a fundamental mode Gaussian beam is shown in Fig. 2, in which $\omega_{0m} = \omega_0 M$ is the width of the multimode Gaussian beam. ω_0 is the width of the fundamental mode Gaussian beam [7]. The distribution of multimode Gaussian beam intensity can be calculated through the weighted average of $I_i(x,z)$, that is,

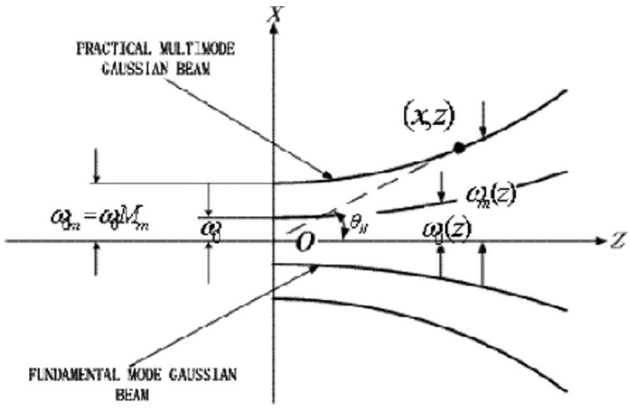

Fig. 2. Relationship between multimode Gaussian beam and fundamental mode Gaussian beam.

$$I_m(x,z) = \sum_{i=0}^{+\infty} C_i I_i(x,z), \tag{1}$$

where C_i is the weight factor,

$$C_i = \frac{2{\omega_0}^2}{{\omega_{0m}}^2 + {\omega_0}^2}\left(\frac{{\omega_{0m}}^2 - {\omega_0}^2}{{\omega_{0m}}^2 + {\omega_0}^2}\right)^i. \tag{2}$$

Each mode beam intensity distribution is shown as

$$I_i(x,z) = A_i H_i^2\left(\frac{\sqrt{2}}{\omega_0(z)}x\right)\exp\left(-2\frac{x^2}{\omega_0(z)^2}\right). \tag{3}$$

In Eq. (3),

$$A_i = 2n_{\text{eff}}\sqrt{\frac{\omega\varepsilon_0}{\beta(\pi {a_m}^2)}}P,$$

$$H_i(x) = (-1)_i e^{x^2}\frac{\partial^i}{\partial x^i}e^{-x^2}$$

is the Hermite polynomial.

On inserting Eqs. (2) and (3) into Eq. (1), we obtained

$$I_m(x,z) \propto P\cdot\sum_{-\infty}^{+\infty}\frac{2{\omega_0}^2}{{\omega_{0m}}^2 + {\omega_0}^2}\left(\frac{{\omega_{0m}}^2 - {\omega_0}^2}{{\omega_{0m}}^2 + {\omega_0}^2}\right)^i \cdot H_i^2\left(\frac{\sqrt{2}}{\omega_0(z)}x\right)\exp\left(-2\frac{x^2}{\omega_0(z)^2}\right). \tag{4}$$

With the linear array working at a current of 4 A, we calculated that the theoretical optical power values P of each individual unit with 100 μm, 150 μm, and 200 μm aperture size are 0.364 W, 0.856 W, and 1.52 W. The corresponding beam quality factors measured with a lens transform method authenticated by the International Organization for Standardization (ISO) [8] are 35, 47, and 61. The corresponding near-field waists of the units are 7.66 μm, 8.88 μm, and 10.12 μm by inserting from the waist of the fundamental mode Gaussian beam 1.296 μm [9] into $\omega_{0m} = \omega_0 M$. After inserting the above parameters of each unit into Eq. (4), we simulate the superimposed near-field distribution as shown in Fig. 3.

A Fourier transform is made to the near-field Eq. (4) to get the far-field distribution expression, that is,

$$I_m(\theta,z) \propto P\sum_{-\infty}^{+\infty}\frac{2{\omega_0}^2}{{\omega_{0m}}^2 + {\omega_0}^2}\left(\frac{{\omega_{0m}}^2 - {\omega_0}^2}{{\omega_{0m}}^2 + {\omega_0}^2}\right)^i \times H_i^2\left(\frac{\sqrt{2}}{\omega_0(z)}tg(\theta)z\right)\exp\left(-2\frac{tg^2(\theta)z^2}{\omega_0(z)^2}\right). \tag{5}$$

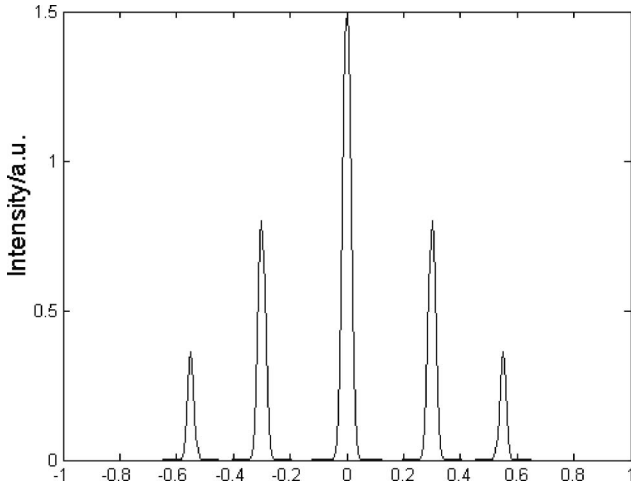

Fig. 3. Near-field distribution of the nonuniform linear array.

The superimposed far-field distribution at a distance of 5 cm from the lasing aperture is shown in Fig. 4. The solid line represents the superimposed far-field distribution of the linear array, while the other lines correspond to the far fields of each element. It is concluded that the superimposition of the far-field distribution of the nonuniform linear array creates a Gaussian distribution of the beam profile, which is beneficial for the applications of fiber coupling and a high brightness laser source.

4. Results and Discussion

The dimensions and the L-I-V characteristics of the nonuniform linear array are shown in Figs. 1 and 5. A maximum output power of 880 mW and a corresponding average optical power density of 1 kW/cm^2 at an injected current of 4 A are obtained. At this current, the slope efficiency is 0.3 W/A with a low threshold of 0.56 A and a differential resistance of 0.09 Ω. The inset of the far-field image in Fig. 5 indicates a Gaussian far-field intensity distribution.

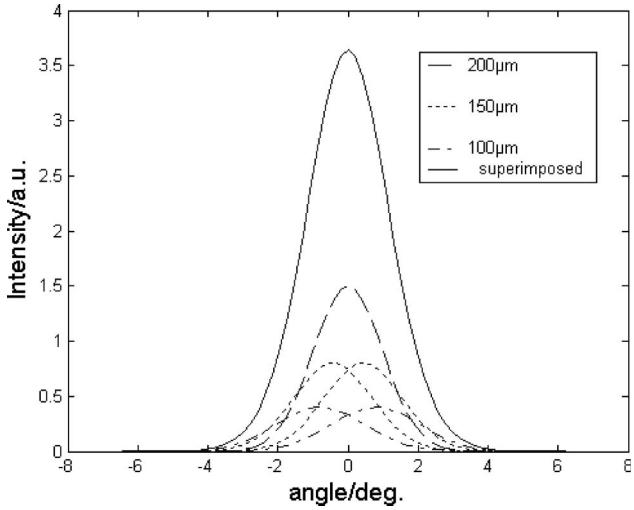

Fig. 4. Superimposed far-field distribution (solid line) of the linear array and far-field distribution of each element (dashed line).

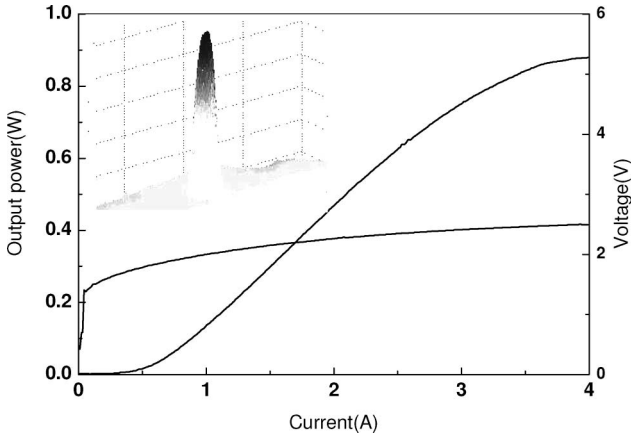

Fig. 5. Dependence of output power and forward voltage on the current of a nonuniform linear array.

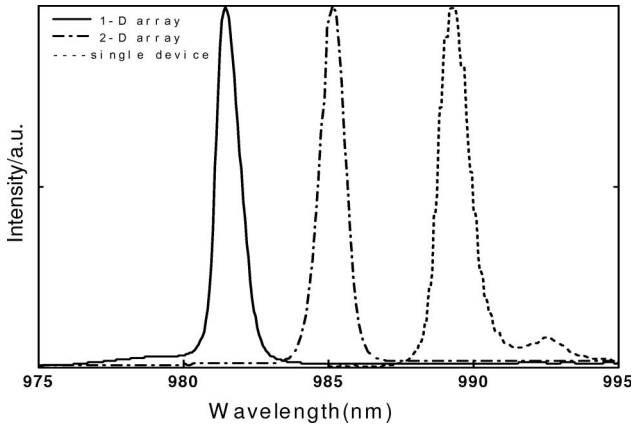

Fig. 7. Lasing spectra of the three kinds of devices.

As a comparison, the conventional 2D array can only provide a far field with a periodic intensity or a quasi top-hat distribution [10].

The performance of the nonuniform linear array is compared with a single device of 300 μm aperture and a 4 × 4, 2D array with an element aperture of 50 μm and center to center spacing of 250 μm, which have been fabricated and reported early in [11,12]. These three kinds of device have the same lasing area. The dependences of the output power and the applied voltage on the current of the three devices are presented in Fig. 6. Thermal rollover is observed for all three devices. The maximum output power of the linear array (880 mW) is a little lower than a single device (950 mW), but higher than a 2D array (690 mW). The reason can be ascribed as follows. The significant thermally induced lens effect in an array device will convert more optical power into heat, which might lead to lower power conversion efficiency compared with a single VCSEL device. In addition, the high density of the 4 × 4, 2D array makes the cross talk of the thermal effect more serious than in the linear array. The larger aperture and wider distance of each element in the linear array make it easy for heat extraction, which results in higher output power than the 4 × 4, 2D array. In addition, the linear array shows the smallest threshold current of the three devices. A single device with a large aperture size needs more current to fill in the active area to reach the lasing condition, so it has a higher threshold current than an array. For the 4 × 4 array, more generation of heat will consume a large number of carriers, so the linear array has a better performance in the threshold current.

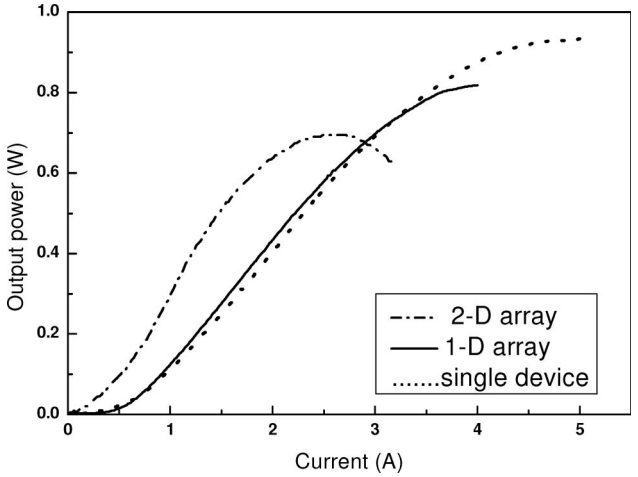

Fig. 6. Dependence of the output power on the current of the three kinds of devices.

The linear array shows less redshift among the three devices, as shown in Fig. 7. The asymmetric current injection due to the large lasing area and the severe thermal effect result in a large redshift in a single device and a 2D array, respectively.

The far-field images and lasing intensity distributions of these three kinds of device are depicted in Fig. 8. For the single device, a ring shaped far field is induced by the nonuniform current distribution across the active region under low current. With increasing current, a peak appears at the symmetry axis with several weak peaks around. With increasing injected current far beyond threshold current, the far field becomes a bright spot with a much narrower divergent angle. For a 2D array, the emissions of individual elements superimpose and form a periodic intensity distribution with a series of peaks at far field. On the contrary, for a linear array with optimized center to center spacing and diameters of elements, the intensity superimposition of the beams from all elements creates an intensity maximum at the symmetry axis with a divergent angle of below 20° in the whole range of operating currents from 0 A to 6 A, which is in good agreement with theoretical simulation. A good balance among the output power, the power conversion efficiency, and the operation current is obtained through this configuration of a nonuniform array, which can provide high brightness and high efficiency for the applications of fiber coupling, solid laser pumping, and free space communication.

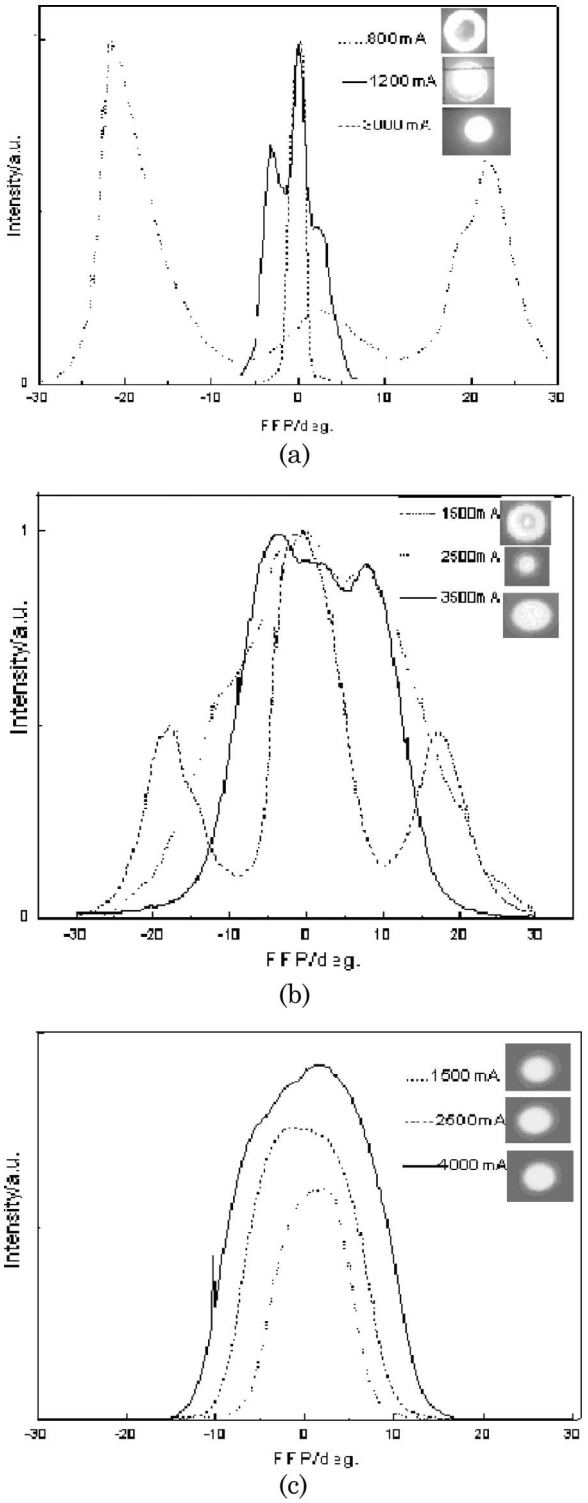

Fig. 8. Far-field images and lasing intensity distribution of (a) single device, (b) 2D array, and (c) linear array.

5. Conclusion

A nonuniform linear VCSEL array with a high power density of $1\,kW/cm^2$ and a Gaussian far-field distribution is developed. As a comparison, a conventional 2D array and a single device exhibits a periodic intensity distribution or ring-shaped distribution at far field. The linear array also shows a better performance in the output power, threshold current, lasing spectra, and far-field distribution. Higher optical power with a Gaussian beam profile could be expected with integrating more elements in a nonuniform 2D configuration, which provides a good overall power efficiency for applications of high brightness and high coupling efficiency.

This work is supported by the Chinese Academy of Sciences (CAS) Innovation Program under contracts 60636020, 60676034, 60706007, 60577003, and 60876036 and by the National Science Foundation (NSF).

References

1. D. Wiedenmann, R. King, C. Jung, R. Jager, and R. Michalzik, "Design and analysis of single-mode oxidized VCSELs for high-speed optical interconnects," IEEE. J. Sel. Top. Quantum Electron. **5**, 503–511 (1999).
2. R. S. Geels, S. W. Corzine, and L. A. Coldren, "InGaAs vertical cavity surface emitting lasers," IEEE J. Quantum Electron. **27**, 1359–1367 (1991).
3. F. Mederer, R. Jager, P. Schnitzer, H. Unold, M. Kicherer, K. J. Ebeling, M. Natomi, and R. Yoshida, "Multi-Gigabit/s graded-index POF data link with butt-coupled single-mode InGaAs VCSEL," IEEE Photon. Technol. Lett. **12**, 199–201 (2000).
4. R. Jäger, M. Grabherr, C. Jung, R. Michalzik, G. Reiner, B. Weigl, and K. J. Ebeling, "57% wallplug efficiency oxide-confined 850 nm wavelength GaAs VCSELs," Electron. Lett. **33**, 330–331 (1997).
5. N. Ueki, H. Nakayama, J. Sakurai, A. Murakami, H. Otoma, Y. Miyamoto, M. Yamamoto, R. Ishii, M. Yoshikama, and T. Nakamura, "Complete polarization control of 12 × 8-bit matrix-addressed oxide-confined vertical-cavity surface-emitting laser array," Jpn. J. Appl. Phys. **40**, L33–L35 (2001).
6. M. C. Amann, M. Ortsiefer, R. Shau, and J. Rosskopf, "Vertical-cavity surface-emitting laser diodes for telecommunication wavelengths," Proc. SPIE **4871**, 123–129 (2002).
7. P. Li, J. Sun, H. Chen, and W. Guo, "Study of the model of laser diode emitted beam based on multimode Gaussian distribution," Proc. SPIE **6824**, 68241H (2007).
8. "Lasers and laser-related equipment. Test methods for laser beam parameters, beam widths, divergence angle and beam propagation factor," ISO 11146 (International Organization for Standardization, 1996).
9. S. A. Riyopoulos, D. Dialetis, J. Liu, and B. Riely, "Generic representation of active cavity VCSEL eigenmodes by optimized waist Gauss–Laguerre modes," IEEE J. Sel. Top. Quantum Electron. **7**, 312–327 (2001).
10. J.-F. Seurin, C. L. Ghosh, V. Khalfin, A. Miglo, G. Xu, J. D. Wynn, P. Pradhan, and L. A. D'Asaro, "High-power high-efficiency 2D VCSEL arrays," Proc. SPIE **6908**, 690808 (2008).
11. Y. Sun, Z. Jin, Y. Ning, L. Qin, C. Yan, G. Luo, G. Tao, Y. Liu, L. Wang, D. Cui, H. Li, and Z. Xu, "Fabrication and experimental characterization of high power bottom-emitting VCSELs," Opt. Precision Eng. **12**, 449–453 (2004).
12. T. Li, Y. Ning, Y. Sun, C. Wang, J. Liu, Y. Liu, and L. Wang, "High-power InGaAs VCSELs single devices and 2-D arrays," J. Luminescence **122–123**, 571–573 (2007).